INTERNATIONAL JOURNAL FOR NUMERICAL METHODS IN FLUIDS
*Int. J. Numer. Meth. Fluids* 2009; **59**:475–493
Published online 9 July 2008 in Wiley InterScience (www.interscience.wiley.com). DOI: 10.1002/fld.1810

REVIEW

# Local Heaviside-weighted LRPIM meshless method and its application to two-dimensional potential flows

Iraj Saeedpanah*,† and E. Jabbari

*Department of Civil Engineering, Iran University of Science and Technology, P.O. Box 16765-163, Narmak, Tehran, Iran*

SUMMARY

In this paper, the local radial point interpolation meshless method (LRPIM) is used for the analysis of two-dimensional potential flows, based on a local-weighted residual method with the Heaviside step function as the weighting function over a local subdomain. Trial functions are constructed using radial basis functions. The present method is a truly meshless method based only on a number of randomly located nodes. Integration over the subdomains requires only a simple integration cell to obtain the solution. No element matrix assembly is required and no special treatment is needed to impose the essential boundary conditions. The novelty of the paper is the use of a local Heaviside weight function in the LRPIM, which does not need local domain integration and integrations only on the boundary of the local domains are needed. Effects of the sizes of local subdomain and interpolation domain on the performance of the present method are investigated. The behavior of shape parameters of multiquadrics has been systematically studied. Two numerical tests in groundwater and fluid flows are presented and compared with closed-form solutions and finite element method. The results show that the use of a local Heaviside weight function in the LRPIM is highly accurate and possesses no numerical difficulties. Copyright © 2008 John Wiley & Sons, Ltd.

Received 30 June 2006; Revised 17 February 2008; Accepted 22 February 2008

KEY WORDS: LRPIM meshless method; heaviside step function; multiquadric; radial basis function; local weak form; local quadrature domain

## 1. INTRODUCTION

The finite element method (FEM) has been established as a very powerful numerical technique for the analysis of space domain problems having arbitrary shapes. However, it has some drawbacks. It has been observed that in the FEM, mesh generation is a far more time-consuming and expensive

*Correspondence to: Iraj Saeedpanah, Department of Civil Engineering, Iran University of Science and Technology, P.O. Box 16765-163, Narmak, Tehran, Iran.
†E-mail: saeedpanah@iust.ac.ir, i_s_panah@yahoo.com

task than the assembly and solution of the finite element equations. Moreover, there are certain classes of problems for which FEM is difficult, or even impossible to apply, such as problems with discontinuities, moving boundaries, or severe deformations [1]. For such problems, it has become necessary to find the methods that may be slightly more expensive from the viewpoint of computer time but require less time in the preparation of data. Recently, a class of new methods, known as meshless methods, has been developed. The so-called mesh-free methods have become a very attractive alternative for computer modeling and simulation of problems in engineering and sciences. These methods do not require a mesh to discretize the problem domain. The approximation functions are constructed entirely using a set of scattered nodes, and no element or connectivity of the nodes is needed.

Various meshless methods belonging to this family are smooth particle hydrodynamics [2, 3], diffuse element method [4], reproducing kernel particle method [5], the method of finite spheres [6], free mesh method [7], local boundary integral equation method [8], the partition of unity method [9], element-free Galerkin (EFG) method [10–16], natural element method [17] and natural neighbor Galerkin method [18], the meshless local Petrov–Galerkin (MLPG) method [19, 20] and the local radial point interpolation meshless method (LRPIM) [21–25]. The methods based on global weak form (GWF) showed promising results, but they suffer a drawback. They are not truly meshless methods, i.e. they are 'meshless' only in terms of the interpolation of the field variables and have to use background cells to integrate a weak form over the problem domain. The MLPG method does not need any 'element' or 'mesh' for either field interpolation or background integration, and any non-element interpolation scheme such as the moving least square [26], the PUM or the radial basis functions (RBFs) can be used for trial and test functions. The flexibility in choosing the size and the shape of the local subdomain leads to a convenient formulation in dealing with non-linear problems. Particularly, the local Heaviside-weighted MLPG together with RBFs interpolation [27, 28] showed great promise for steady problems because only a regular boundary integral along the edges of subdomains is involved and no special treatment on imposing essential boundary condition is needed. On methods that use the local boundary integration, there is also a new and interesting development by Liu *et al.* [29]. Liu *et al.* [30–32] have found that the integrations (in the local domain or on the boundary of the domain) for all the internal nodes are not necessary for many problems, and the integrations are needed only for the local domain of the nodes near the problem domain. This led to the development of the mesh-free weak–strong method for both solid and fluid problems.

The LRPIM meshless method developed was first presented by Liu *et al.* [21–25]. Trial functions are constructed using RBFs. Liu was the first researcher who used arbitrary shape parameters in RBFs. As LRPIM can be regarded as a local-weighted residual method, the weight function plays an important role in the performance of this method. We have used the truly meshless LRPIM for solving two-dimensional potential flows using a local Heaviside weight function. In the LRPIM, the function over the solution domain requires only a set of nodes and does not require element connectivity. Integration over the subdomains requires only a simple integration cell to obtain the solution. The results are obtained for a model problem and compared with the results of exact method and FEM.

## 2. RBF INTERPOLATION

The local interpolation using RBFs [33, 34] enables trial functions to pass through the actual values of the unknown variables at scattered nodes. The later one is used in this study.



DOI: 10.1002/fld

A continuous function $u(x)$ defined in a domain $\Omega$ discretized by a set of nodes can be interpolated from the neighboring nodes of a point $x_Q$ using RBFs as

$$u^h(x, x_Q) = \sum_{i=1}^{n} R_i(x)\overline{a}_i(x_Q) = R^{\mathrm{T}}(x)a(x_Q) \tag{1}$$

where $R_i(x)$ is the RBF in the space coordinates $x^{\mathrm{T}} = [y, z]$, $n$ is the number of nodes in the neighborhood (refers to the domain of interpolation) of $x_Q$, and $\overline{a}_i(x_Q)$ are the coefficients for $R_i(x)$, respectively, corresponding to the given point $x_Q$. It should be noted that the number $n$ of the neighboring nodes of $x_Q$ is less than or equal to the total number of nodes in the global problem domain $n$ depending on the size of the support domain specified. The vectors are defined as

$$\overline{a} = [\overline{a}_1, \overline{a}_2, \overline{a}_3, \ldots, \overline{a}_n]^{\mathrm{T}} \tag{2}$$

$$R^{\mathrm{T}} = [R_1(x), R_2(x), R_3(x), \ldots, R_n(x)]^{\mathrm{T}} \tag{3}$$

The radial distance function in a vertical two-dimensional domain is a function of Euclidean distance $r$ defined as

$$r_i = [(x - x_i)^2 + (y - y_i)^2]^{1/2} \tag{4}$$

The radial distance function transforms a multiple-dimensional problem into one dimension. Enforcing the interpolation to pass through all $n$-scattered points within the point $x_Q$ support domain leads to the following set of equations for the coefficients $\overline{a}_i(x_Q)$:

$$u_k = u(x_k, y_k) = \sum_{i=1}^{n} \overline{a}_i(x_Q) R_i(x_k, y_k), \quad k = 1, 2, 3, \ldots, n \tag{5}$$

which can be expressed in matrix form as follows:

$$R_Q a = U_s \tag{6}$$

where $U_s = [u_1, u_2, u_3, \ldots, u_n]$ and $R_Q$ is the interpolation matrix of rank $(n \times n)$ as follows:

$$R_Q = R_Q^{\mathrm{T}} = \begin{bmatrix} R_1(r_1) & R_2(r_1) & \ldots & R_n(r_1) \\ R_2(r_2) & R_2(r_2) & \ldots & R_n(r_2) \\ \vdots & \vdots & \ddots & \vdots \\ R_1(r_n) & R_2(r_n) & \ldots & R_n(r_n) \end{bmatrix} \tag{7}$$

The coefficients can be obtained as

$$a = R_Q^{-1} U_s \tag{8}$$

where $R_Q^{-1}$ is the inverse matrix of $R_Q$.

Finally, the interpolation can be expressed as

$$u^h(x) = R^{\mathrm{T}}(x) R_Q^{-1} U_s = \Phi(x) U_s \tag{9}$$



DOI: 10.1002/fld

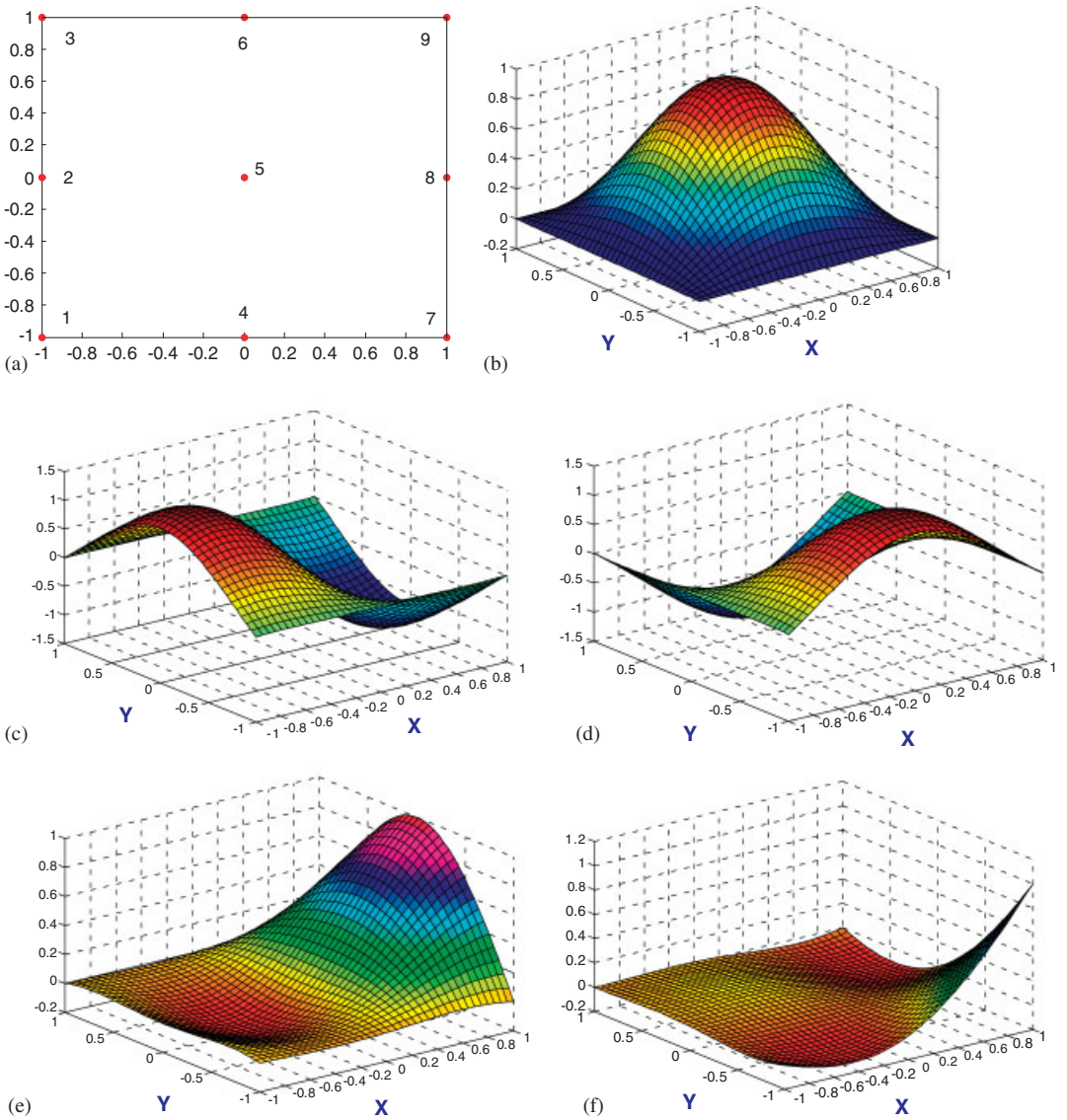


Figure 1. Shape functions for two-dimensional domain (9 nodes): (a) domain and nodal arrangement; (b) shape function of central node (node 5); (c) shape function derivative in the $x$ direction of central node; (d) shape function derivative in the $y$ direction of central node; (e) shape function for an edge node (node 8); and (f) shape function for a corner node (node 7).

where the matrix of shape functions $\Phi(x)$ is defined as

$$\begin{aligned}\Phi(x) &= [R_1(x), R_2(x), \ldots, R_k(x), \ldots, R_n(x)]R_Q^{-1} \\ &= [\phi_1(x), \phi_2(x), \ldots, \phi_k(x), \ldots, \phi_n(x)] \end{aligned} \tag{10}$$



DOI: 10.1002/fld

in which

$$\phi_k(x) = \sum_{i=1}^{n} R_i(x) S_{ik}^a \tag{11}$$

and $S_{ik}^a$ is the $(i,k)$ element of the matrix $R_Q^{-1}$. The derivatives of $\phi_k(x)$ can be obtained as follows:

$$\frac{\partial \phi_k}{\partial x} = \sum_{i=1}^{n} \frac{\partial R_i}{\partial x} S_{ik}^a \tag{12}$$

$$\frac{\partial \phi_k}{\partial y} = \sum_{i=1}^{n} \frac{\partial R_i}{\partial y} S_{ik}^a \tag{13}$$

There are several RBFs available. The most important three RBFs consisting multiquadrics (MQ), Gaussian (EXP), and thin plate splines (TPS) are as follows:

$$R_i(x,y) = (r_i^2 + (\alpha_c d_c)^2)^q, \quad \alpha_c \geqslant 0 \text{ (MQ)} \tag{14}$$

$$R_i(x,y) = (r_i)^\eta \log r_i \text{ (TPS)} \tag{15}$$

$$R_i(x,y) = \mathrm{e}^{-c^2 r_i^2} \text{ (EXP)} \tag{16}$$

where $q$, $\alpha_c$, and $\eta$ are the shape parameters that are used for fine tuning. The MQ-RBF is studied in this article. The partial derivatives of the MQ-RBF can be obtained as follows:

$$\begin{aligned} \frac{\partial R_i}{\partial x} &= 2q(r_i^2 + (\alpha_c d_c)^2)^{q-1}(x - x_i) \text{ (MQ)} \\ \frac{\partial R_i}{\partial y} &= 2q(r_i^2 + (\alpha_c d_c)^2)^{q-1}(y - y_i) \text{ (MQ)} \end{aligned} \tag{17}$$

Figure 1 shows typical shape functions for a two-dimensional problem using MQ basis with an interpolation domain containing $3 \times 3$ nodes only in a $[-1,1] \times [-1,1]$ $x$–$y$ space. The shape parameters are chosen to be $\alpha_c = 1.42$ and $q = 1.03$. For better compatibility, the dimensionless size of support domain is $\alpha_s = 3.5$. All the shape functions satisfy the delta function property and as is obvious both shape function and its derivatives are smooth functions and unlike FEM need no smoothing technique. It should be noted that the 9-node domain in Figure 1 is in the sense of a local domain surrounded by other nodes and the shape functions have zero value for any points immediately outside the local domain. If the global domain is discretized with these 9 nodes, the local domain is equal to the global domain.

## 3. LOCAL WEAK FORM

Meshless methods that use a weak form of equations are categorized into GWF and local weak form (LWF). EFG and RKPM are examples of global weak methods over the entire domain $\Omega$ whereas LRPIM uses LWF of equations over a local subdomain of arbitrarily shaped $\Omega_Q$ called quadrature domain, which is located entirely inside the global domain $\Omega$. This is the most distinguishing feature of the LRPIM meshless method. In comparison to the GWF methods, the LWF will provide a clear



DOI: 10.1002/fld

concept for a local meshless integration of the weak form, which does not need any background integration cells over the entire domain. In addition, it will lead to a natural way to construct the global stiffness matrix: not through the integration over a contiguous mesh or by assembly of the stiffness matrices of the elements in the mesh but through the integration over local subdomains. Consider the following two-dimensional Poisson equation, which is the governing equation in this paper, in a domain $\Omega$ bounded by $\Gamma$:

$$\frac{\partial^2 u}{\partial x^2}+\frac{\partial^2 u}{\partial y^2}=P(x,y) \tag{18}$$

where $u$ is the field variable and $P$ is the body force field. The domain $\Omega$ is enclosed by $\Gamma=\Gamma_u\cup\Gamma_q$, with boundary conditions. The boundary conditions are given as follows:

$$\frac{\partial u}{\partial n}=\nabla\cdot\mathbf{n}=\overline{q} \quad \text{on } \Gamma_q \tag{19a}$$

$$u=\overline{u} \quad \text{on } \Gamma_u \tag{19b}$$

where $\Gamma_q$ is the boundary with predefined flux, $\Gamma_u$ is the essential boundary, $n$ is the unit outward normal to the domain $\Omega$, and $q$ is the flux over the boundary.

A LWF of Equation (18), over a local subdomain $\Omega_Q$ bounded by $\Gamma_Q$, can be obtained using the weighted residual method:

$$\int_{\Omega_Q} W\left(\frac{\partial^2 u}{\partial x^2}+\frac{\partial^2 u}{\partial y^2}-P(x,y)\right)\mathrm{d}\Omega=0 \tag{20}$$

where $W$ is the test function. It should be noted that there are neither Lagrange multipliers nor penalty parameters introduced in Equation (20) because, as mentioned earlier, the shape functions satisfy the Kronecker delta property and, hence, the essential boundary condition can be imposed directly, as done in FEM. Using the divergence theorem in Equation (20) and imposing the natural boundary condition, the following local symmetric weak form (LSWF) can be obtained:

$$\int_{\Omega_Q}(W_{,x}u_{,x}+W_{,y}u_{,y})\,\mathrm{d}\Omega-\int_{\Gamma_{Qi}}W\frac{\partial u}{\partial n}\,\mathrm{d}\Gamma-\int_{\Gamma_{Qu}}W\frac{\partial u}{\partial n}\,\mathrm{d}\Gamma=-\int_{\Omega_Q}W\,P\,\mathrm{d}\Omega+\int_{\Gamma_{Qq}}W\overline{q}\,\mathrm{d}\Gamma \tag{21}$$

where $\Gamma_{Qq}$ is a part of $\Gamma_Q$, over which the natural boundary condition is specified; $\Gamma_{Qu}$ is the intersection of $\Gamma_Q$ and the essential boundary $\Gamma_u$; $\Gamma_{Qi}$ is the internal part of $\Gamma_Q$ on which no boundary condition is specified, as shown in Figure 2. For a quadrature domain located entirely within the global domain, there is no intersection between $\Gamma_Q$ and $\Gamma$, and the integrals over $\Gamma_{Qu}$ and $\Gamma_{Qq}$ vanish. The support subdomain $\Omega_Q$ of a node $x_i$ is a domain in which $W_i(x)\neq 0$. An arbitrarily shaped support domain can be used. Generally, a circle or rectangular support domain is used for convenience. For an internal node, the integration can be done numerically within the local domain. For a node on or near the boundary, only a local mesh is required. Therefore, no global background mesh is required. Different local test functions can be used in the weak form (21), which leads to different ways to construct the global stiffness matrix [35, 36]. The Heaviside step function is used as the test function in this research. Thus, the LWF (21) can be



DOI: 10.1002/fld

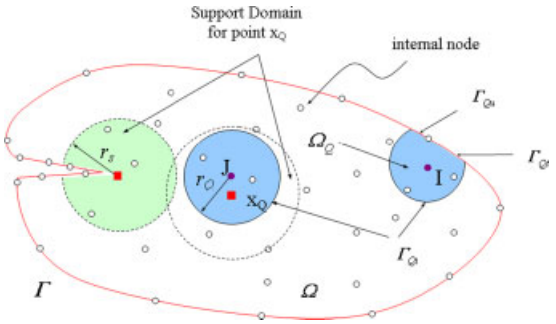


Figure 2. The support domain and the quadrature domain in constructing the discretized equation for node I.

rewritten as

$$\int_{\Gamma_{Qi}} \frac{\partial u}{\partial n}\,\mathrm{d}\Gamma + \int_{\Gamma_{Qu}} \frac{\partial u}{\partial n}\,\mathrm{d}\Gamma = \int_{\Omega_Q} P\,\mathrm{d}\Omega - \int_{\Gamma_{Qq}} \overline{q}\,\mathrm{d}\Gamma \tag{22}$$

It can be seen that the domain integral in the weak form (22) is avoided and only the regular boundary integral along the boundaries of subdomains is involved. The LSWF, Equation (22), gives one algebraic equation relating all. Therefore, we need as many local domains $\Omega_Q$ as the number of nodes in the global domain.

## 4. DISCRETIZATION AND NUMERICAL IMPLEMENTATION

The LWF is based on the quadrature domain $\Omega_Q$ centered on each nodal point $x_i$. The shapes of quadrature domains can be chosen arbitrarily, such as a circle or a rectangle for two-dimensional problems. If the nodal points $x_i$ and the support domain of the nodal shape functions for the trial function are given, then the subdomain weak form can be constructed for each quadrature domain $\Omega_Q$. There is no restriction on the size of the quadrature domains or the support domains of the nodal shape functions for the trial function. The quadrature domains can be taken to be different from the supports of the nodal trial shape functions. Provided the union of all quadrature domains covers the global domain, the equilibrium equation and the boundary conditions will be satisfied in the global domain and on its boundary. For certain cases, as will be shown in this paper, the union of all subdomains can be smaller than the global problem domain. However, the union of all supports of the nodal trial shape functions must cover the global domain in all cases, so that the connections between different quadrature domains can always be secured.

Assume that the problem domain $\Omega$ is represented by properly scattered nodes. The unknown variable $u$ in this LSWF is approximated by the nodal shape functions (10). To obtain the discrete equations from the LSWF (22), the RBF interpolation (9) is adopted to approximate the trial function $u$. Substitution of Equation (9) into Equation (22) for all nodes leads to the following discretized system of linear equations:

$$[K]\{u\} = \{f\} \tag{23}$$



DOI: 10.1002/fld

where $[K]$ and $\{f\}$ are the 'stiffness' matrix and the 'load' vector, respectively, defined as

$$K_{IJ} = \int_{\Gamma_{Qi}} \phi_{J,x} n_x + \phi_{J,y} n_y \, d\Omega + \int_{\Gamma_{Qu}} \phi_{J,x} n_x + \phi_{J,y} n_y \, d\Omega \tag{24}$$

$$f_I = \int_{\Omega_Q} P(x, y) \, d\Omega - \int_{\Gamma_{Qq}} \overline{q} \, d\Omega \tag{25}$$

The Gauss quadrature is employed in each local subdomain centered at node $x_i$. For each Gauss quadrature point $x_Q$, RBF is performed to obtain the integrand. Therefore, for a node $x_i$, there are two local domains: the test function domain $\Omega_{\text{te}}$ (same as the local subdomain $\Omega_Q$) for $W_i \neq 0$ (size $r_Q$) and the interpolation domain $\Omega_s$ for $x_Q$ (size $r_s$). Figure 2 shows the quadrature domain $\Omega_Q$ of a node $x_i$ and the support domain $\Omega_s$ for a Gauss point $x_Q$. These two domains are independent and defined as

$$r_Q = \alpha_Q d_c, \quad r_s = \alpha_s d_c \tag{26}$$

where $\alpha_s$ and $\alpha_Q$ are dimensionless coefficients and $d_c$, known as characteristic length, is the shortest spacing between node $I$ and its closest neighbor nodes or the global boundary, whichever is smaller. Parameters including shape parameters of RBFs and parameters related to LRPIM (support and subdomain size) should be tuned. According to Professor G. R. Liu's recommendation the shape parameters are chosen to be $\alpha_c = 1.42$ and $q = 1.03$. For better compatibility, the dimensionless size of support domain is $\alpha_s = 3.7$ [35, 36].

As mentioned before, because the shape functions constructed by RBFs possess the delta function property, the essential boundary condition can be implemented easily and the terms in the row of the matrix $K$ for the nodes on the essential boundary need not be computed, which reduces the computing cost.

## 5. NUMERICAL TESTS

In this section, numerical results will be presented to illustrate the implementation and convergence of the LRPIM meshless method. Systematic parametric studies are also performed on shape parameters of the extended MQ. In all examples, the body forces are set to be 0. For the purpose of error estimation and convergence studies, the $L_2$ norm is defined as follows:

$$\|L_2\| = \left\{ \int_{\Omega} (u^{\text{LRPIM}} - u^{\text{exact}})^{\text{T}} (u^{\text{LRPIM}} - u^{\text{exact}}) \, d\Omega \right\}^{1/2} \tag{27}$$

where $u^{\text{LRPIM}}$ and $u^{\text{exact}}$ are the field variables computed by the LRPIM method and the closed-form solution.

## 6. GROUNDWATER FLOW

One of the important contributions, illustrating the power of mathematical tools, was Toth's [37, 38] work on the influence of water-table configuration on flow in groundwater basins. His analytical approach allowed him to test different water-table configurations and determine what types of



DOI: 10.1002/fld

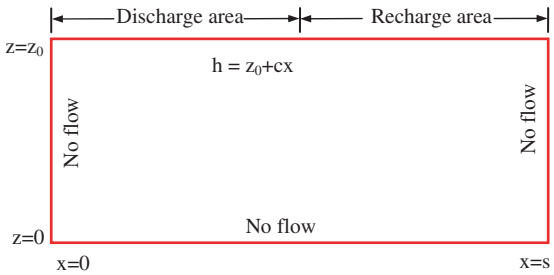


Figure 3. A two-dimensional region with boundary conditions for regional flow.

groundwater flow patterns emerged. The case that Toth considered was flow in a basin with a linear sloping water-table as shown in Figure 3. Toth [37] formulated this problem for a two-dimensional cross section oriented parallel to the likely direction of regional flow in a groundwater basin.

The boundary conditions have no flow boundary condition at left, right, and bottom boundaries:

$$\left.\frac{\partial h}{\partial x}\right|_{x=0}=0, \quad \left.\frac{\partial h}{\partial x}\right|_{x=s}=0, \quad \left.\frac{\partial h}{\partial z}\right|_{z=0}=0 \tag{28}$$

However, the hydraulic head is identified at the top boundary:

$$h=z_0+cx \tag{29}$$

where $z_0$ is the hydraulic head at $x=0$ and $c$ is the slope of water-table. In this study, $c=0.05$ and $z_0=100$ are adopted. An analytical solution to the problem was given by Toth [37] as follows:

$$h=z_0+\frac{cs}{2}-\sum_{m=0}^{\infty}\frac{\cos[(2m+1)\pi x/s]\cosh[(2m+1)\pi z/s]}{(2m+1)^2\cosh[(2m+1)\pi z_0/s]} \tag{30}$$

Figure 4 shows the results for $\alpha_c=5.25$, $q=1.98$ by MQ RBF in a $22*11$ nodal domain. In all computations, $\alpha_Q=0.85$ and $\alpha_s=3.5$ are considered; the number of segments on quadrature domain boundary is 4; and GQ6 scheme is employed for integration in each direction.

### *6.1. Shape parameters of MQs*

The choice of shape parameters for MQ basis function has been well studied by a number of researchers [33, 34, 39–44]. Optimal values of $q=1.03$ and $\alpha_c=1.42$ were identified in [33, 34], where they used RBFs in EFG. We will further determine the optimal shape parameters in the Toth groundwater problem in this section. In the study, we limit our investigation on the shape parameters to $q$ ranging from $-0.5$ to 2.25 and $\alpha_c$ ranging from 0.3 to 7. Taking $\alpha_Q=0.85$ and $\alpha_s=3.5$, the variation of $L_2$ norm errors of head with shape parameters is given in Figure 5.

It can be seen in Figure 5(a) that $q=0.98$, 1.03, and 1.98 leads to better accuracy. It should be noted that $q$ cannot be an integer; otherwise the moment matrix will be singular. From Figure 5(b), it can be seen that, for most $q$ values, the accuracy is sensitive to the shape parameter $\alpha_c$. However, for the values $q=1.03$ and 0.98, despite higher accuracy, the accuracy is less sensitive to $\alpha_c$ in the range $[4.8, 6.2]$. As shown in Figure 5(b), we cannot find $\alpha_c=1.42$ to be an optimal value but $\alpha_c=5.25$ to be optimal. Consequently, we will further employ MQ-RBF with $q=0.98$ and $\alpha_c=5.25$.



DOI: 10.1002/fld

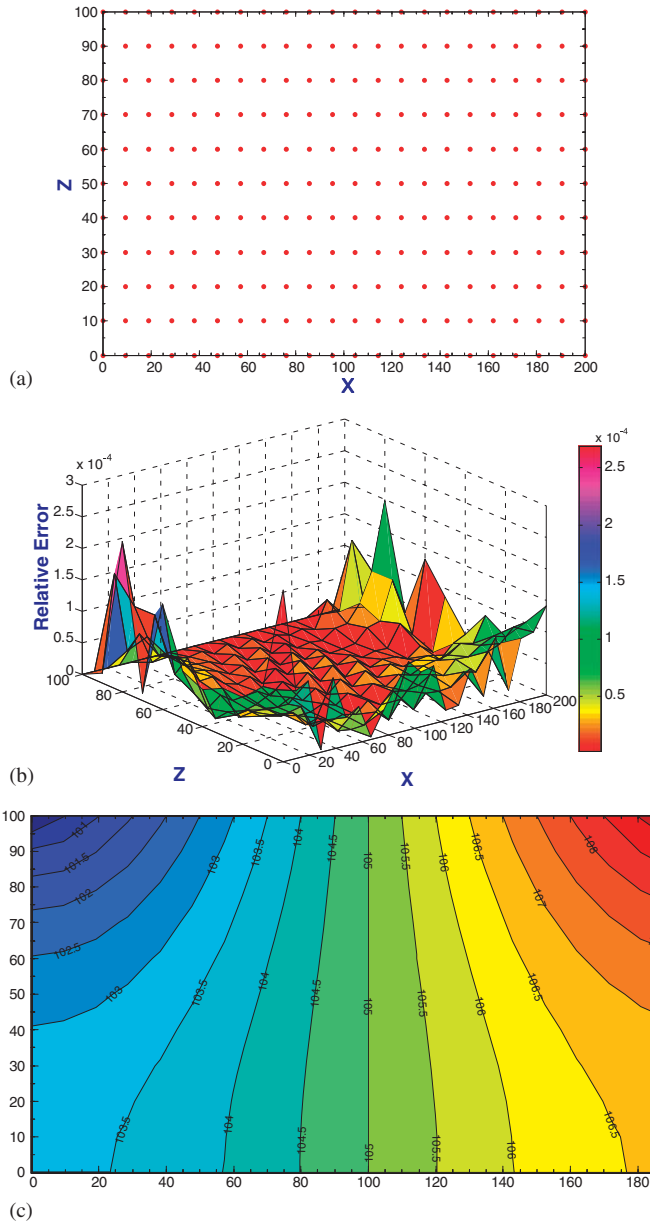


Figure 4. LRPIM results: (a) domain and nodal arrangements; (b) relative error; and (c) approximated function head contour.



DOI: 10.1002/fld

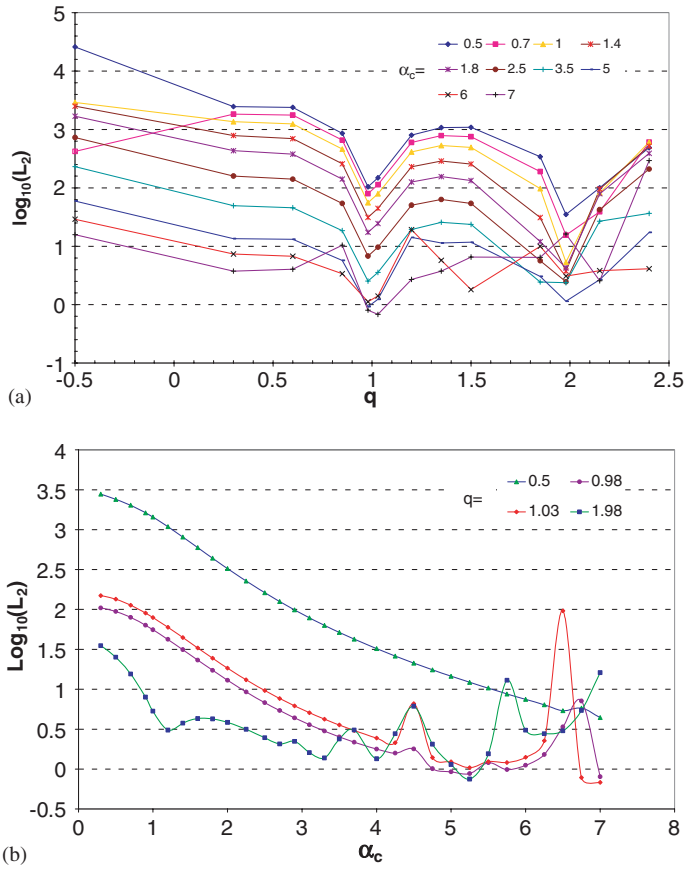


Figure 5. Effect of shape parameters $q$, $\alpha_c$, $L_2$ norm error for multiquadric RBF: (a) shape parameter $q$ and (b) shape parameter $\alpha_c$.

### 6.2. *Effects of the size of subdomain*

In subdomain-based meshless methods, the size of the quadrature domain used will affect the accuracy of the solution. In this paper, we limit the quadrature domain size as being larger than zero and less than one. It should be noted that when $\alpha_Q = 0$ the present method converts to the point collocation method. Limiting the quadrature domain size as less than one makes integration of Equation (22) for internal nodes simpler because there is no intersection between the internal quadrature domains and the global boundary. When $\alpha_s$ is less than 0.5, there is no overlap between quadrature domains, and quadrature domains overlap each other when $\alpha_s$ is between 0.5 and 1.

Quadrature domains with different sizes are examined and the $L_2$ errors of potential head are plotted in Figure 6 with $q = 0.5, 0.98, 1.03$, and 1.98. The size of the interpolation domain is taken as $\alpha_s = 3.5$ and $\alpha_c$ is taken as 5.25. It can be seen that excellent accuracy is obtained when $\alpha_Q$ varies from 0.1 to 1 for $q = 0.98$, 1.03, and 1.98. However, in most calculations except those in this subsection we use the parameter as $\alpha_Q = 0.75$, allowing overlap between the quadrature domains, which may give more reliable results for most cases.



DOI: 10.1002/fld

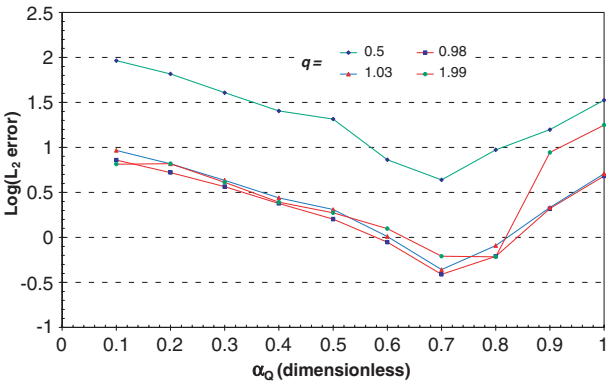


Figure 6. Effect of quadrature domain parameters $\alpha_Q$ for MQ-RBF.

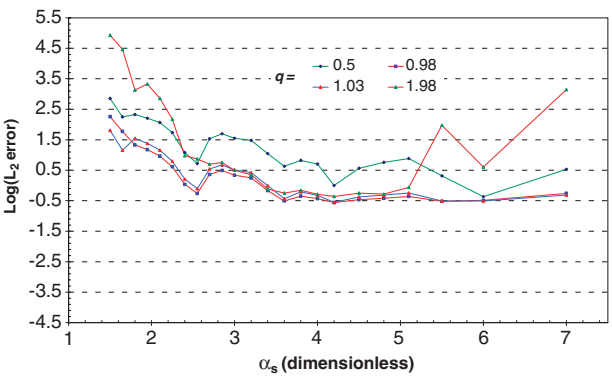


Figure 7. Influence of the support domain size $\alpha_s$ for MQ-RBF for different values of $q$.

### 6.3. *Effects of the size of interpolation domain*

The size of the support (or interpolation) domain plays a very important role in all meshless methods. It is related to both the accuracy of the solution and the computational efficiency of the method. The errors of $L_2$ norms for $\alpha_s = 1.5$–7 are obtained and plotted in Figure 7 for $q = 0.5, 0.98, 1.03$, and 1.98, respectively.

It can be seen that if $\alpha_s$ is less than 2, the results are not acceptable simply because there are not enough nodes to perform interpolation. For $q = 1.98$, the results are less satisfying due to ill-conditioning of moment matrix. When $\alpha_s$ is larger than 2, the results of $q = 0.5$ are acceptable and also $q = 0.5$ is of higher accuracy out of $[2.5, 5.1]$ than $q = 1.98$. The results of $q = 1.03$ and 0.98 show good satisfaction in the range $[3.5, 7]$. In implementation, as the value of $\alpha_s$ increases, the bandwidth of moment matrix $A$ increases and, consequently, leads to inefficient computation. In addition, a small bandwidth means lower complexity, but larger errors.

It is worth noting that the research by Liu and Gu [21–23] showed large errors with $\alpha_s > 3.5$ and recommended $\alpha_s = 1.5$–3 for defining the interpolation domain size (15–40 nodes used in an interpolation domain). In this research, we examined interpolation domain sizes $\alpha_s$ up to 7 (more



DOI: 10.1002/fld

than 150 nodes included for performing interpolation), and there is no problem at all when the interpolation size is larger than 3.5 up to 5. As shown, a value of $\alpha_s = 4.2$ may be optimal for $q = 1.03$ and 0.98. In advance, $\alpha_s = 4.2$ is adopted for further computation.

### 6.4. *Convergence rate and effect of node density*

The convergence with mesh refinement of the present method is studied in this section and compared with the Lagrangian triangular FEM results. The results of convergence rates are shown in Figure 8.

Four values $0.5, 0.98, 1.03$, and $1.98$ were used for the shape parameter $q$. In this study, we choose $\alpha_c = 5.25$, $\alpha_Q = 0.75$ and $\alpha_s = 4.2$, which were identified as optimal values. Six different node densities of $45(5*9)$, $120(8*15)$, $276(12*23)$, $630(18*35)$, $1127(24*47)$, and $2016(32*63)$ are used. The $L_2$ norms are evaluated using $20*10(200)$ cells with $6*6(36)$ Gauss quadrature points for each cell. The error norms with the convergence rates are given in Table I. It can be seen that both the convergence rates of $q = 1.03$ and 0.98 are the best, and the convergence rate

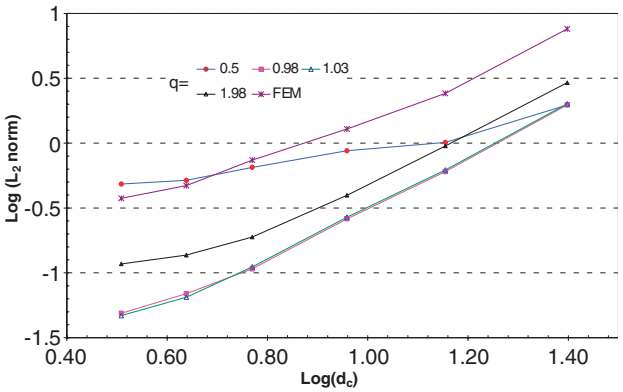


Figure 8. Convergence rates in $L_2$ norm for MQ-RBF and FEM.

Table I. $L_2$ norm with convergence rates for FEM and LRPIM.

| | LRPIM | | | | |
|---|---|---|---|---|---|
| Elements/nodes | $q = 0.5$ | $q = 0.98$ | $q = 1.03$ | $q = 1.98$ | FEM |
| $5*9$ | 0.2947 | 0.2945 | 0.30289 | 0.46567 | 0.8803 |
| $8*15$ | 0.0047513 | −0.21916 | −0.20691 | −0.021665 | 0.3841 |
| $12*23$ | −0.0585 | −0.58382 | −0.57044 | −0.40262 | 0.1092 |
| $18*35$ | −0.186498 | −0.96885 | −0.95405 | −0.72369 | −0.1311 |
| $24*47$ | −0.287316 | −1.1609 | −1.1879 | −0.86332 | −0.32731 |
| $32*63$ | −0.31572 | −1.3115 | −1.3293 | −0.931082 | −0.42572 |
| Rate of convergence | 0.6671 | 1.8353 | 1.8717 | 1.6201 | 1.4592 |



DOI: 10.1002/fld

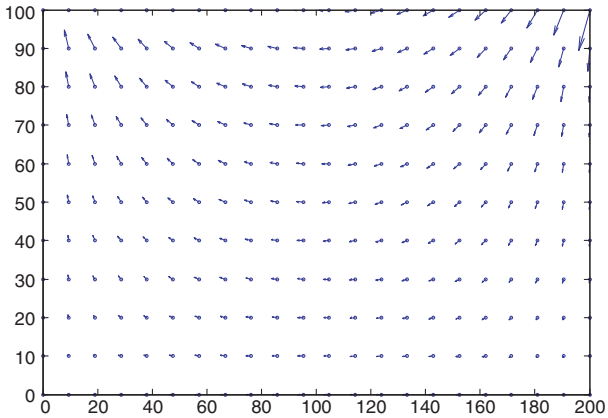


Figure 9. The velocity vectors of groundwater.

of $q=1.98$ is slightly better than that of the FEM results. The velocity field can be obtained as

$$\mathbf{V}=(u,v)=-\frac{\partial h}{\partial x_i}=-\sum_{J=1}^{n_t}\frac{\partial \phi^J}{\partial x_i}h^J, \quad i=1,2 \tag{31}$$

As long as the shape functions are smooth enough, unlike FEM, no smoothing technique is required. The velocity vectors are illustrated in Figure 9.

## 7. TWO-PLATE FLOW

Consider the flow over two infinite plates that intersect at the origin with 135° angle as shown in Figure 10.

The analytical solution for the flow potential is

$$\phi=\tfrac{3}{4}(r^{4/3})\cos(\tfrac{4}{3}\theta) \tag{32}$$

where $(r,\theta)$ are the usual polar coordinates. The Dirichlet boundary conditions are considered for top and right edges, whereas Neumann boundary conditions are considered for left and bottom edges. The optimal parameters investigated in previous sections, i.e. $\alpha_c=5.25$, $\alpha_Q=0.75$, $\alpha_s=4.2$, and $q=1.03$, are considered for the problem. Figure 11 shows the results for a domain with 145 nodes. The relative error is plotted in Figure 11(c), which is defined as

$$r_e=\frac{\phi^{\mathrm{LRPIM}}-\phi^{\mathrm{exact}}}{\phi^{\mathrm{exact}}} \tag{33}$$

where $\phi^{\mathrm{LRPIM}}$ and $\phi^{\mathrm{exact}}$ are equipotential lines computed by the LRPIM method and the closed-form solution.

In order to study convergence rates, the $L_2$ norm is calculated and compared with the FEM results, which is shown in Figure 12.



DOI: 10.1002/fld

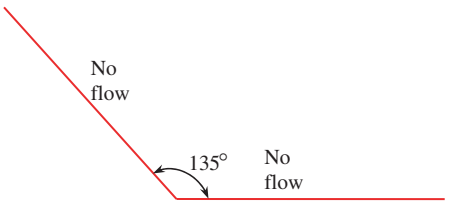


Figure 10. The domain and boundary conditions for two-plate flow.

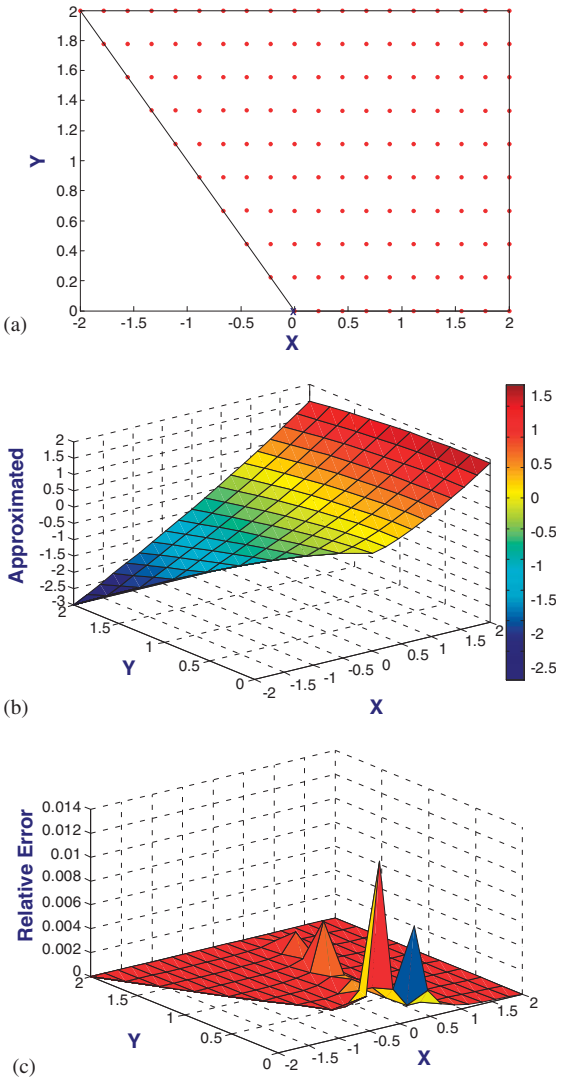


Figure 11. Two-plate flow: (a) domain and nodal arrangements; (b) approximated function; and (c) relative error.



DOI: 10.1002/fld

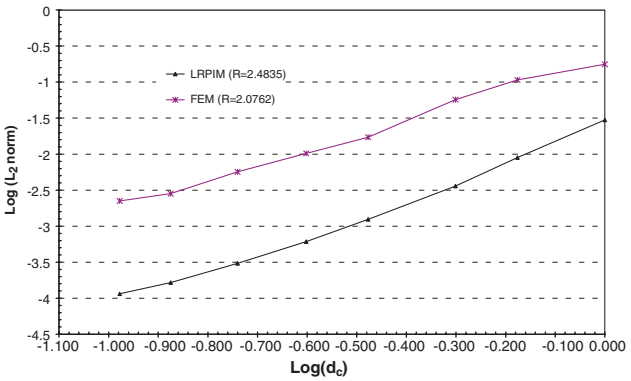


Figure 12. Convergence rates in $L_2$ norm for LRPIM and FEM.

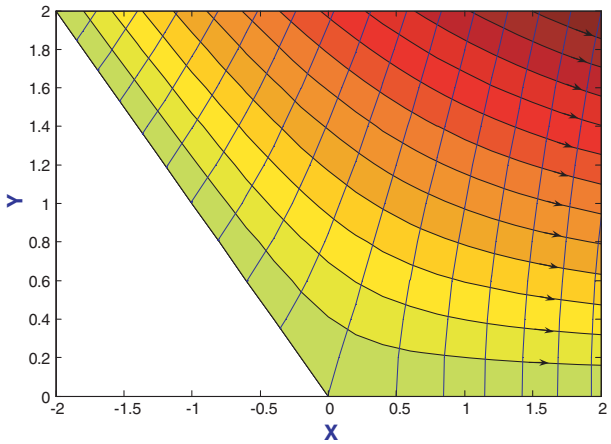


Figure 13. Flownet obtained from LRPIM.

As shown, despite higher accuracy of the LRPIM meshless method, the convergence rate is also higher than that of FEM.

The streamlines and equipotential lines are plotted in Figure 13.

The velocity vectors can be calculated as

$$\mathbf{V} = \nabla\phi \tag{34}$$

where $\phi$ is equipotential lines and $\mathbf{V}$ is the velocity vectors.

## 8. CONCLUSIONS

A meshless method based on the local radial point interpolation meshless method (LRPIM) has been presented for solving the problems of two-dimensional potential flows. In this meshless



DOI: 10.1002/fld

method, the Heaviside step function is used as the test function and a local interpolation technique using RBFs is used to construct the trial function entirely in terms of a set of scattered nodes. The novelty of the paper is the use of Heaviside weight function in the LRPIM, which does not need local domain integration and only integrations on the boundary of the local domains are needed. The results show that the use of a local Heaviside weight function in the LRPIM is highly accurate and possesses no numerical difficulties. MQ-RBFs were employed and various shape parameters were examined for $q$ and $\alpha_c$. Effects of quadrature domain size and support domain size were investigated with different shape parameters. It can be seen that there is no integration difficulty in the present method, no element matrix assembly is required, and no special treatment is needed to impose the essential boundary conditions. Compared with FEM, the results are of higher accuracy, whereas compared with other meshless methods, the implementation procedure is simple and the computation cost is much lower because of the simple interpolation and the simple way to construct the global stiffness matrix.

## APPENDIX: NOMENCLATURE

| | |
|---|---|
| $\alpha_c, q$ | shape parameters |
| $d_c$ | characteristic length between node $i$ and its neighbor nodes |
| $r_Q$ | radius of the quadrature domain (subdomain) |
| $r_s$ | radius of the support domain |
| $\alpha_Q$ | dimensionless size of quadrature domain |
| $\alpha_c$ | dimensionless shape parameters for MQ ($C/d_c$) |
| $\alpha_s$ | dimensionless size of support domain |
| $u^h(x, y)$ | radial basis function interpolant |
| $n$ | number of nodes in the support domain |
| $h$ | hydraulic head |
| $\Gamma_s$ | boundary of the quadrature domain |
| $\Omega_Q$ | quadrature domain (local subdomain) |
| $\Phi(x)$ | shape function |
| $\psi$ | stream function |

## REFERENCES


1. Zienkievicz OC, Taylor RL. *The Finite Element Method* (4th edn). McGraw-Hill: London, 1991.
2. Monaghan JJ. An introduction to SPH. *Computer Physics Communications* 1988; **48**:89–96.
3. Monaghan JJ. Smooth particle hydrodynamics. *Annual Review of Astronomy and Astrophysics* 1992; **30**:543–574.
4. Nayroles B, Touzot G, Villon P. Generalizing the finite element method; diffuse approximation and diffuse elements. *Computational Mechanics* 1992; **10**:307–318.
5. Liu WK, Jun S, Zhang YF. Reproducing kernel particle methods. *International Journal for Numerical Methods in Fluids* 1995; **20**:1081–1106.
6. De S, Bathe J. The method of finite spheres. *Computational Mechanics* 2000; **25**:329–345.
7. Yagawa G, Yamada T. Free mesh method: a new meshless finite element method. *Computational Mechanics* 1996; **18**:383–386.
8. Zhu T, Zhang JD, Atluri SN. A meshless local boundary integral equation (LBIE) method for solving nonlinear problems. *Computational Mechanics* 1998; **22**:174–186.
9. Babuska I, Melenk JM. The partition of unity method. *International Journal for Numerical Methods in Engineering* 1997; **40**:727–758.




DOI: 10.1002/fld

10. Liu GR, Gu YT. Meshless local Petrov–Galerkin (MLPG) method in combination with finite element and boundary element approaches. *Computational Mechanics* 2000; **26**:536–546.
11. Liu GR, Gu YT. Vibration analyses of 2-D solids by the local point interpolation method (LPIM). *Proceedings of 1st International Conference on Structural Stability and Dynamic*, Taiwan, 7–9 December 2000; 411–416.
12. Liu GR, Gu YT. Coupling of element free Galerkin and hybrid boundary element methods using modified variational formulation. *Computational Mechanics* 2000; **26**(2):166–173.
13. Lu YY, Belytschko T, Gu L. A new implementation of the element free Galerkin method. *Computer Methods in Applied Mechanics and Engineering* 1994; **113**:397–414.
14. Belytschko T, Lu YY, Gu L. Element free Galerkin methods. *International Journal for Numerical Methods in Engineering* 1994; **37**:229–256.
15. Belytschko T, Krongauz Y, Organ D, Liu WK. Smoothing and accelerated computations in the element free Galerkin method. *Journal of Computational and Applied Mathematics* 1996; **74**:111–126.
16. Dolbow J, Belytschko T. An introduction to programming the meshless element-free Galerkin method. *Archives of Computational Methods in Engineering* 1998; **5**:207–241.
17. Sukumar N, Moran B, Belytschko T. The natural element method in solid mechanics. *International Journal for Numerical Methods in Engineering* 1998; **43**:839–887.
18. Sukumar N, Moran B, Yu Semenov A, Belikov VV. Natural neighbour Galerkin methods. *International Journal for Numerical Methods in Engineering* 2001; **50**:1–27.
19. Atluri SN, Zhu T. A new meshless local Petrov–Galerkin (MLPG) approach in computational mechanics. *Computational Mechanics* 1998; **22**:117–127.
20. Atluri SN, Zhu T. A new meshless local Petrov–Galerkin (MLPG) approach to non-linear problems in computer modelling and simulation. *Computer Modeling and Simulation in Engineering* 1998; **3**:187–196.
21. Liu GR, Gu YT. A point interpolation method for two-dimensional solids. *International Journal for Numerical Methods in Engineering* 2001; **50**:937–951.
22. Liu GR, Gu YT. A local point interpolation method for stress analysis of two-dimensional solids. *Structural Engineering and Mechanics* 2001; **11**(2):221–236.
23. Liu GR, Gu YT. A local radial point interpolation method (LR-PIM) for free vibration analyses of 2-D solids. *Journal of Sound and Vibration* 2001; **246**(1):29–46.
24. Liu GR, Yan L, Wang JG, Gu YT. Point interpolation method based on local residual formulation using radial basis functions. *Structural Engineering and Mechanics* 2002; **14**(6):713–732.
25. Gu YT, Liu GR. A boundary radial point interpolation method (BRPIM) for 2D structural analyses. *Structural Engineering and Mechanics* 2003; **15**(5):535–550.
26. Liu X, Liu A. A meshless method based on least-squares approach for steady- and unsteady-state heat conduction problems. *Numerical Heat Transfer B* 2005; **47**(3):257–275.
27. Wang JG, Liu GR. Numerical analysis of Biot's consolidation process by radial point interpolation method. *International Journal of Solids and Structures* 2002; **39**(6):1557–1573.
28. Mukherjee YX, Muknherjee S. Boundary node method for potential problems. *International Journal for Numerical Methods in Engineering* 1997; **40**:797–815.
29. Liu GR, Zhang GY, Dai KY, Wang YY, Zhong ZH, Li YG, Han X. A linearly conforming point interpolation method (LC-PIM) for 2D mechanics problems. *International Journal of Computational Methods* 2005; **2**(4): 645–665.
30. Liu GR, Gu YT. A meshfree method: meshfree weak-strong (MWS) form method, for 2-D solids. *Computational Mechanics* 2003; **33**(1):2–14.
31. Gu YT, Liu GR. A meshfree weak-strong (MWS) form method for time dependent problems. *Computational Mechanics* 2005; **35**(2):134–145.
32. Liu GR, Wu YL, Ding H. Meshfree weak–strong (MWS) form method and its application to incompressible flow problems. *International Journal for Numerical Methods in Fluids* 2004; **46**:1025–1047.
33. Wang JG, Liu GR. A point interpolation meshless method based on radial basis functions. *International Journal for Numerical Methods in Engineering* 2002; **54**(11):1623–1648.
34. Wang JG, Liu GR. On the optimal shape parameters of radial basis functions used for 2D meshless methods. *Computer Methods in Applied Mechanics and Engineering* 2002; **191**:2611–2630.
35. Gu YT, Liu GR. A meshless local Petrov–Galerkin (MLPG) formulation for static and free vibration analyses of thin plates. *Computer Modeling in Engineering and Sciences* 2001; **2**(4):463–476.
36. Atluri SN, Shen S. The meshless local Petrov–Galerkin (MLPG) method: a simple & less-costly alternative to the finite element and boundary element methods. *Computer Modeling in Engineering and Sciences* 2002; **3**:11–51.



DOI: 10.1002/fld

37. Toth J. A theory of ground water motion in small drainage basins in central Alberta. *Journal of Geophysical Research* 1962; **67**:4375–4387.
38. Toth J. A theoretical analysis of ground water flow in small drainage basins. *Journal of Geophysical Research* 1963; **68**:4795–4812.
39. Hardy RL. Multiquadric equations of topography and other irregular surfaces. *Journal of Geophysical Research* 1971; **76**:1905–1915.
40. Hardy RL. Theory and applications of the mutliquadrics—biharmonic method (20 years of discovery 1968–1988). *Computers and Mathematics with Applications* 1990; **19**:163–208.
41. Frank R. Scattered data interpolation: tests of some method. *Mathematics of Computation* 1982; **38**(157):181–200.
42. Carlson RE, Foley TA. The parameter $R^2$ in multiquadric interpolation. *Computers and Mathematics with Applications* 1991; **21**:29–42.
43. Golberg MA, Chen CS, Karur SR. Improved multiquadric approximation for partial differential equations. *Engineering Analysis with Boundary Elements* 1996; **18**:9–17.
44. Rippa S. An algorithm for selecting a good value for the parameter c in radial basis function interpolation. *Advances in Computational Mathematics* 1999; **1**:193–210.



DOI: 10.1002/fld